J|A|C|S
COMMUNICATIONS

Published on Web 09/09/2003

Simultaneous in Situ Total Internal Reflectance Fluorescence/Atomic Force Microscopy Studies of DPPC/dPOPC Microdomains in Supported Planar Lipid Bilayers

James E. Shaw, Andrea Slade, and Christopher M. Yip*

Departments of Biochemistry, Chemical Engineering, and Applied Chemistry, Institute of Biomaterials and Biomedical Engineering, 4 Taddle Creek Road, Toronto, Ontario, Canada, M5S 3G9

Received July 5, 2003; E-mail: christopher.yip@utoronto.ca

The cell membrane represents the interface between the cell and its environment. Understanding molecular interactions that occur at the membrane surface as well as within the membrane and their effect on membrane stability and cellular processes is therefore critical for efforts in proteomics and for the development of novel therapies for the treatment of disease. For example, membrane microdomains, including rafts,[1] are believed to play a critical role in important cellular functions such as signal transduction[2] and membrane trafficking.[3,4] While imaging of these structures by combined fluorescence and scanning probe microscopy has been reported,[5−8] it has been difficult to simultaneously acquire real-time in situ spectral and structural data with submicron resolution. Recent advances in near-field scanning optical microscopy (NSOM) have provided correlated fluorescence and topographic information with ∼30−100 nm resolution;[6,9−11] however, concerns remain about probe−sample interactions, reproducible probe fabrication, operation in liquid environments, image acquisition times, and decoupling of the topographical and optical images.[12] To address these concerns and in support of our studies of membrane protein assemblies and bilayer dynamics by in situ scanning probe microscopy,[13] we have married far-field total internal reflectance (TIRF) with atomic force microscopy (AFM). While combined AFM/TIRF techniques have been used to study force transmission[14] and single-particle manipulation[15] in cells, to the best of our knowledge, this is the first application of this approach to the study of membrane systems.

Supported planar lipid bilayers were prepared by direct vesicle fusion onto freshly cleaved mica of a binary lipid mixture ([1:1] DPPC/dPOPC) containing ∼2 mol % of a fluorescently labeled lipid (NBD-PC, 460/534 nm, Avanti Polar Lipids, Alabaster, AL). The fusion process was conducted in situ using a custom thermostated fluid cell fitted to our AFM. To facilitate domain formation, the liposome solution was heated in situ to ∼60 °C for ∼30 min. All TIRF/AFM imaging was performed at ambient temperature in buffer.

The TIRF/AFM instrument was comprised of a Digital Instruments Nanoscope IIIa Bioscope scanning probe microscope (Santa Barbara, CA) equipped with an extended *z*-range "J" scanner (116 μm × 116 μm maximum lateral scan area) mounted on an Olympus Fluoview 500 confocal microscope equipped with an Olympus TIRF accessory (10 mW Ar-ion (488 nm) laser (Melles Griot, CA); Olympus 60 × 1.45 NA TIRF objective). The TIRF images were acquired simultaneously using a cooled CCD camera (CoolSNAP HQ, Roper Scientific, AZ). As the TIRF/epi-fluorescence/confocal optical paths are independent, we can rapidly interconvert between these different optical imaging modalities. All AFM images were acquired in tapping mode using 120 μm oxide-sharpened silicon nitride V-shaped cantilevers installed in a combination contact/tapping liquid cell.

In situ fusion of the NBD-PC doped DPPC/dPOPC liposomes onto the mica surface resulted in the formation of two-phase planar lipid bilayers with the taller domains extending ∼1.5 nm above the shorter domains (Figure 1a). Control studies of DPPC/dPOPC bilayers containing no fluorophores exhibited similar phase separation (data not shown). There was very good correspondence between the TIRF and AFM images with bright regions in TIRF correlating to darker, or shorter, regions in AFM (Figure 1b). Because NBD-PC is known to partition into the more disordered phase when two lipid phases coexist,[8,16−18] this suggests that the shorter domains are the less ordered regions of the bilayer, in agreement with previous AFM studies of binary lipid systems.[8,19] At ambient room temperature (∼26 °C), the taller domains therefore correspond to the gel-phase DPPC ($T_m \approx 41$ °C), while the shorter domains are the fluid-phase dPOPC ($T_m \approx -36$ °C) regions. The ∼1.5 nm topographic difference between the two lipid phases has been attributed to changes in the tilt of the lipid acyl chain.[6,20−23] Comparison between feature dimensions measured by AFM and those measured by TIRF revealed an ∼15% difference in lateral size (Figure 1c). For this work, we assumed that the decay of the TIRF signal corresponds to the point spread function of fluorophores located at the domain boundaries. There was no significant optical interference from the supporting mica substrate. While our TIRF/AFM system could resolve individual fluorescent domains separated by at least ∼275 nm (as determined by AFM), the true spatial resolution of the combined technique remains untested (Figure 1a). Close inspection revealed that some features in the TIRF image are not present in the AFM image (and vice versa). Variations in fluorescence intensity at domain boundaries may reflect localized mixing of the DPPC and dPOPC lipids (Figure 1b). Poor resolution of domain edges by TIRF may also be attributed to its inherent diffraction-limited nature. While differences in fluorescence intensity in the bulk suggest a nonuniform fluorophore distribution in a given phase, the time necessary to acquire the different images may also play a role. At a typical scan rate of 2 Hz, a 512 × 512 pixel AFM image would be acquired in ∼4 min, as compared with the 30 fps imaging rate of the TIRF camera system. As such, the TIRF system provides an excellent means of visualizing, and capturing, events that occur on very short, approximately millisecond time scales. Real-time TIRF imaging did reveal changes in the distribution of fluorescence not attributable to localized photobleaching,

10.1021/ja0370894 CCC: $25.00

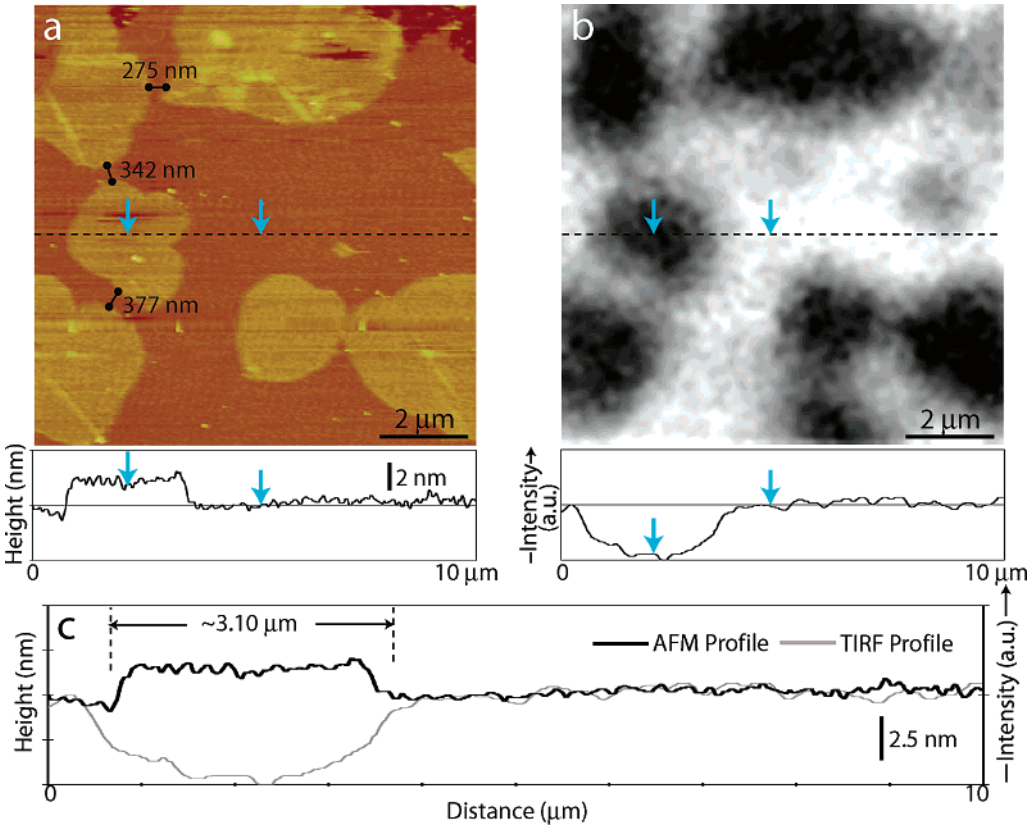

Figure 1. Combined AFM/TIRF imaging. (a) Tapping mode AFM image of a 2% NBD-PC/DPPC/dPOPC lipid bilayer with the taller gel-phase DPPC domains extending ~1.5 nm above the shorter fluid-phase dPOPC domains. (b) TIRF image of the same area (gray scale indicates fluorescence intensity). Bright areas correlate to shorter fluid regions of the bilayer. *Z*-scale: $a = 30$ nm. Scale bar: $a, b = 2$ μm. (c) AFM/TIRF cross-section overlay. The TIRF and AFM images were not captured on the same pixel scale.

suggesting rearrangement within the lipid bilayer on the TIRF time scale (data not shown).

In contrast to NSOM, the combination of AFM and far-field optical techniques is particularly compelling. Decoupling the optical and scanning probe microscopies ensures that the time resolution of the optical measurements is independent of the imaging rate of the AFM and that all of the high-resolution multimodal imaging capabilities afforded traditional AFM are retained. Because TIRF imaging relies on evanescent wave excitation, fluorescence is limited to structures within ~100 nm of the surface. As such, background fluorescence from the bulk solution and backscattering of the excitation source from the AFM cantilever are eliminated. This preliminary work has demonstrated the feasibility of an integrated total internal reflectance/atomic force microscopy imaging platform for functional imaging of supported planar lipid bilayers. We are now using this coupled approach, including TIRF spectroscopy, to characterize membrane protein assemblies.

Acknowledgment. This work was supported by CIHR, NSERC, CFI, OIT, and ORDCF. C.M.Y. is the Canada Research Chair in Molecular Imaging. J.E.S. and A.S. acknowledge support from OGS (J.E.S.), Walter C. Summer Foundation (J.E.S.), and NSERC (A.S.).

References

(1) Simons, K.; Ikonen, E. *Nature* **1997**, *387*, 569−572.
(2) Cinek, T.; Horejsi, V. *J. Immunol.* **1992**, *149*, 2262−2270.
(3) Simons, K.; van Meer, G. *Biochemistry* **1988**, *27*, 6197−6202.
(4) Brown, D. A.; Rose, J. K. *Cell* **1992**, *68*, 533−544.
(5) Ohler, B.; Revenko, I.; Husted, C. *J. Struct. Biol.* **2001**, *133*, 1−9.
(6) Hollars, C. W.; Dunn, R. C. *Biophys. J.* **1998**, *75*, 342−353.
(7) Takamoto, D. Y.; Lipp, M. M.; von Nahmen, A.; Lee, K. Y.; Waring, A. J.; Zasadzinski, J. A. *Biophys. J.* **2001**, *81*, 153−169.
(8) McKiernan, A. E.; Ratto, T. V.; Longo, M. L. *Biophys. J.* **2000**, *79*, 2605−2615.
(9) Yuan, C.; Johnston, L. J. *J. Microsc.* **2002**, *205*, 136−146.
(10) Horiuchi, Y.; Yagi, K.; Hosokawa, T.; Yamamoto, N.; Muramatsu, H.; Fujihira, M. *J. Microsc.* **1999**, *194*, 467−471.
(11) Shiku, H.; Dunn, R. C. *J. Microsc.* **1999**, *194*, 455−460.
(12) Kolodny, L. A.; Willard, D. M.; Carillo, L. L.; Nelson, M. W.; Van Orden, A. *Anal. Chem.* **2001**, *73*, 1959−1966.
(13) Slade, A.; Luh, J.; Ho, S.; Yip, C. M. *J. Struct. Biol.* **2002**, 137.
(14) Mathur, A. B.; Truskey, G. A.; Reichert, W. M. *Biophys. J.* **2000**, *78*, 1725−1735.
(15) Nishida, S.; Funabashi, Y.; Ikai, A. *Ultramicroscopy* **2002**, *91*, 269−274.
(16) Worthman, L. A.; Nag, K.; Davis, P. J.; Keough, K. M. *Biophys. J.* **1997**, *72*, 2569−2580.
(17) Akamatsu, S.; Bouloussa, O.; To, K. W.; Rondelez, F. *Phys. Rev. A* **1992**, *46*, R4504−R4507.
(18) Knobler, C. M. *Science* **1990**, *249*, 870−874.
(19) Giocondi, M. C.; Pacheco, L.; Milhiet, P. E.; Le Grimellec, C. *Ultramicroscopy* **2001**, *86*, 151−157.
(20) Yang, X. M.; Xiao, D.; Xiao, S. J.; Lu, Z. H.; Wei, Y. *Phys. Lett. A* **1994**, *193*, 195−198.
(21) Hollars, C. W.; Dunn, R. C. *J. Phys. Chem. B* **1997**, *101*, 6313−6317.
(22) Masai, J.; ShibataSeki, T.; Sasaki, K.; Murayama, H.; Sano, K. *Thin Solid Films* **1996**, *273*, 289−296.
(23) Yang, X. M.; Xiao, D.; Xiao, S. J.; Wei, Y. *Appl. Phys. A: Mater.* **1994**, *59*, 139−143.

JA0370894